Stretchable, High-*k* Dielectric Elastomers through Liquid-Metal Inclusions

*Michael D. Bartlett, Andrew Fassler, Navid Kazem, Eric J. Markvicka, Pratiti Mandal, and Carmel Majidi**

Soft electronic systems capable of sensing, actuating, and energy harvesting are key components for emerging applications in wearable electronics, biocompatible machines, and soft robotics.[1–5] Traditionally, the electronic properties of rubbery polymers like silicones, polyurethanes, or copolymers such as styrene–ethylene–butylene–styrene are tailored by adding 10–30% by volume of inorganic fillers such as Ag powder, Ag-coated Ni microspheres, structured carbon black (CB), exfoliated graphite, carbon nanotubes, $BaTiO_3$, TiO_2, or other metallic, carbon-based, or ceramic micro-/nanoparticles.[6–12] Although rigid particles have been incorporated into silicones, urethanes, and acrylate-based elastomers to increase their dielectric constant,[13] the loadings required to achieve significant electric property enhancement can degrade the mechanical properties of these soft and stretchable material systems.[10,14–16] The inherently rigid nature of the inorganic filler particles creates a dramatic compliance mismatch with the soft, stretchable elastomer matrix that leads to internal stress concentrations, delamination, and friction that increases bulk rigidity, reduces extensibility, and results in inelastic stress–strain responses that can limit long-term durability at the mesoscale.[16,17] One approach to reduce this compliance mismatch is to use fluid fillers. This has recently been investigated by Style et al. where ionic-liquid inclusions modified the mechanical response of soft elastomers, but electrical properties were not investigated.[18]

Dr. M. D. Bartlett, Dr. A. Fassler, Prof. C. Majidi
Soft Machines Lab
Department of Mechanical Engineering
Carnegie Mellon University
Pittsburgh, PA 15213, USA
E-mail: cmajidi@andrew.cmu.edu

N. Kazem
Soft Machines Lab
Department of Civil and Environmental Engineering
Carnegie Mellon University
Pittsburgh, PA 15213, USA

E. J. Markvicka
Soft Machines Lab
The Robotics Institute
Carnegie Mellon University
Pittsburgh, PA 15213, USA

P. Mandal
Laboratory for Transport Phenomena in Energy Systems
Department of Mechanical Engineering
Carnegie Mellon University
Pittsburgh, PA 15213, USA

DOI: 10.1002/adma.201506243

Here, we incorporate liquid-metal (LM) microdroplets into hyperelastic materials to create all soft matter systems with exceptional electro–elasto properties (**Figure 1**a–c). The integration of LM microdroplets increases the dielectric constant to over 400%, displays a low dielectric dissipation factor, and can be stretched to many times their original length (Figure 1d). This approach eliminates the internal compliance mismatch of rigid fillers and thus preserves the mechanics of the host material, offering a unique combination of low mechanical rigidity and a high dielectric constant (Figure 1e). These liquid-metal embedded elastomers (LMEEs) can be tailored to match the elastic and rheological properties of soft synthetic materials and biological tissue to enable signal transduction, rigidity tuning, and a rich set of other functionalities for biocompatible machines (artificial organs) and electronics (artificial skin and nervous tissue).

Composites are prepared by mixing the LM (eutectic Ga–In (EGaIn) alloy (75% Ga/25% In, by weight) with uncured liquid silicone (Ecoflex 00–30, Smooth-On) or polyurethane (Vytaflex 30, Smooth-On) at volume loadings (ϕ) of LM from 0% to 50% (see the Experimental Section for preparation details). EGaIn is selected as the LM due to its low melting point (MP = 15 °C), high electrical conductivity ($\sigma = 3.4 \times 10^6$ S m^{-1}), low viscosity (η = 2 mPa s), and low toxicity (compared to Hg).[20,21] Additionally, EGaIn oxidizes in air to form a ≈1–3 nm thick Ga_2O_3 skin that allows the liquid droplets to be broken apart and dispersed in solution without the need for emulsifying agents. The microstructure of the EGaIn–silicone composite (ϕ = 50%) is investigated with top-down optical microscopy (Figure 1b) and through nondestructive 3D X-ray imaging using a nano-computed tomographic (CT) scanner (Figure 1c; Figure S1 and Video S1 of the Supporting Information for 3D animation). Together, these two levels of imaging show a disordered but statistically uniform dispersion of droplets and the absence of percolating networks that could result in electrical conductivity or shorting. The microdroplets are also generally ellipsoidal shaped with dimensions measured through 2D particle analysis on the order of ≈4–15 µm (Figure S2 and S3 and Table S1 of the Supporting Information). Because the LMEE composite is a thermoset with a long working time (≥30 min), multiple fabrication techniques can be used to pattern liquid-metal materials, including 3D printing, soft lithography, laser ablation, or stencil lithography techniques.[22] Thin films can also be prepared and, as an example, a stencil patterned EGaIn–silicone specimen is presented in Figure 1d. The electrical polarizability of the LMEEs is crucial for their use as soft, stretchable electronic components. **Figure 2**a presents a plot of effective relative permittivity ε_r^* versus ϕ for an EGaIn–silicone composite at a

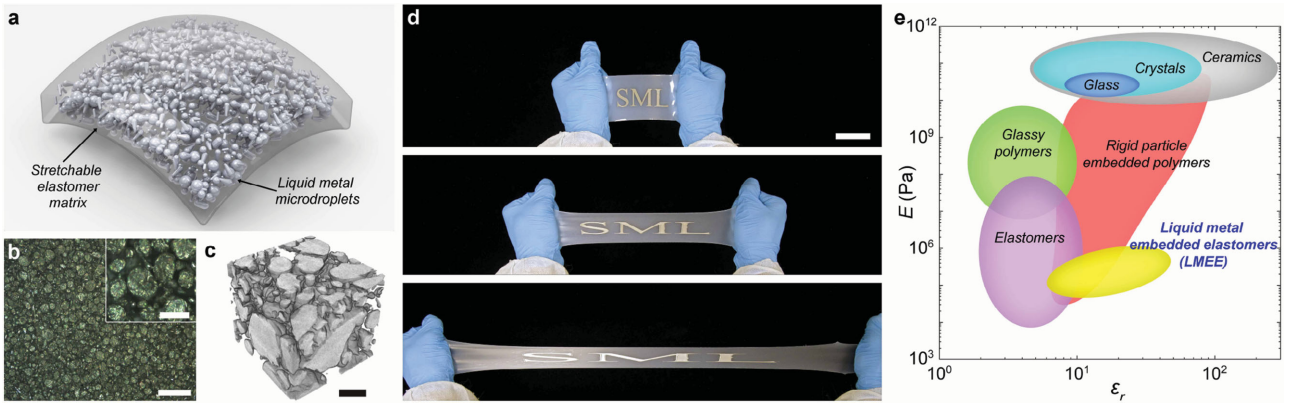

Figure 1. Stretchable, high-*k* dielectrics based on LMEEs. a) Material schematic showing the dispersion of liquid-metal drops in a flexible and stretchable elastomer matrix. b) Top-down optical microscopy images of the $\varphi = 50\%$ silicone LMEEs at different length scales. Scale bar, 100 μm and inset 25 μm. c) Nano-CT scan showing the 3D microstructure of the LMEE. Scale bar, 25 μm. d) Photographs demonstrating the patterning and stretchability of the silicone LMEEs from 0% (top) to 250% (middle) to 500% (bottom) strain. Scale bar, 5 cm. e) Plot of elastic modulus versus dielectric constant for a variety of insulating materials,[13,19] showing the unique combination of low modulus and high dielectric constant of LMEEs.

frequency of 100 kHz and 0% strain. The plot shows that as the concentration of LM increases, the effective relative permittivity increases nonlinearly. For the silicone system, the effective relative permittivity of the sample with $\phi = 50\%$ increases to over 400% as compared to the unfilled system over the entire 1–200 kHz frequency range (Figure 2b). In order to evaluate the ability of the dielectric to store charge, we measure its dissipation factor (D) for the same range of frequencies (Figure 2c). Also called the loss tangent, D corresponds to the ratio of electrostatic energy dissipated to that stored in the dielectric.[13] For LMEEs, the dissipation factor is measured to be similar to or less than that of the unfilled material ($D < 0.1$) and well within the threshold for dielectric functionality. In contrast, many high-*k* composites enhanced with conductive particulates (such as Ag, Al, and CB) become lossy and demonstrate large D values due to non-negligible electrical conductivity at volume fractions on the order of 30%.[8]

To quantitatively understand the increase in relative permittivity, effective medium theory (EMT) can be used to understand the dependency of electro–elasto properties on composition and microstructure. We use a general analytic theory by Nan et al.[23] that allows for inclusions with ellipsoidal shapes with principal dimensions $r_1 = r_2$ and r_3, where the effective relative permittivity ε_r^* can be written as:

$$\varepsilon_r^* = \varepsilon_{rm} \frac{1 + \left\{ \frac{1 - L_{11}}{L_{11}} (1 - \langle \cos^2 \theta \rangle) + \frac{1 - L_{33}}{L_{33}} (\langle \cos^2 \theta \rangle) \right\} \phi}{1 - \phi} \quad (1)$$

Here L_{11} and L_{33} are geometrical factors dependent on the particle shape and are given by:

$$L_{11} = \frac{p^2}{2(p^2 - 1)} - \frac{p}{2(p^2 - 1)^{3/2}} \cosh^{-1} p, \text{ for } p > 1, \quad (1a)$$

$$L_{33} = 1 - 2L_{11}$$

where ε_{rm} is the matrix relative permittivity at $\phi = 0\%$, $p = r_3/r_1$ is the aspect ratio of the ellipsoids, and θ is the angle between the axis along which permittivity is being calculated and the principal axis corresponding to the dimension r_3. For our materials, the average aspect ratio of the LM inclusions measured through particle analysis is $p = 1.49 \pm 0.36$ (Table S1, Supporting Information) and $\langle \cos^2\theta \rangle = 1/3$ for randomly orientated ellipsoids.

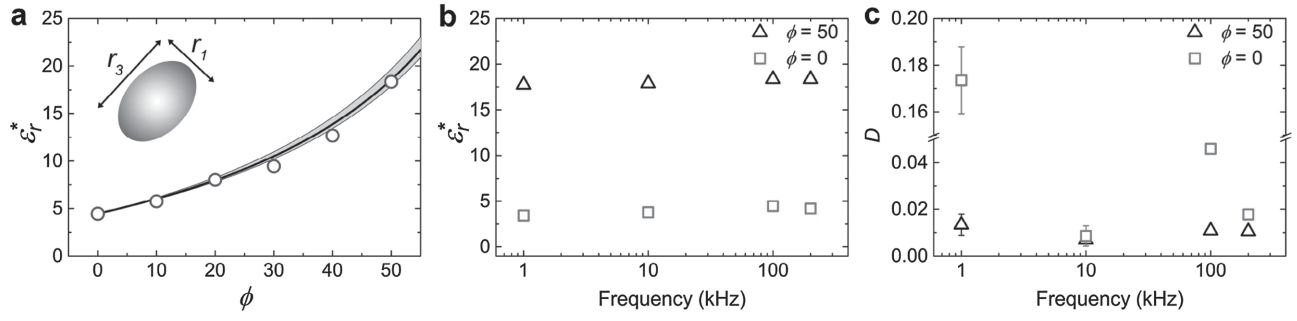

Figure 2. Design and evaluation of silicone LMEE dielectric properties. a) Plot of relative permittivity at 100 kHz frequency versus volume fraction loading of liquid metal (φ) in the elastomer, the line is the theoretical prediction of Equation (1) with $p = 1.49 \pm 0.36$ and the shaded region is ±1 s.d. in p. b) Plot of dielectric constant as a function of testing frequency for $\varphi = 0\%$ and $\varphi = 50\%$ showing an increase of over 400% for the filled system relative to the unfilled system. c) Plot of dielectric dissipation factor as a function of testing frequency showing the low dissipation of the LMEEs. Error bars = ±1 s.d. and error bars smaller than the symbol size are omitted.

Adv. Mater. **2016**,
DOI: 10.1002/adma.201506243

In Figure 2a, the solid curve is the effective relative permittivity, ε_r^*, as a function of ϕ as predicted by Equation (1) and the shaded region represents ±1 s.d. to capture the polydispersity in particle aspect ratio. Although Nan et al. is based on multi-scattering theory and neglect interparticle interactions, the theoretical prediction is still in very good agreement with the experimental data using only experimentally measured parameters. Other potential EMT models for a two-phase material with a dilute suspension of spherical particles include the Maxwell–Garnett (MG) and Bruggeman formulations.[24–26] In particular, we also find good agreement between our data and the MG model (Figure S4, Supporting Information), even though the MG model assumes spherical particles. This suggests that the relatively low aspect ratio ($p = 1.49 \pm 0.36$) of the LM inclusions does not have a large influence on the dielectric response.

The mechanical behavior of the LMEEs is studied under tensile loading for ϕ ranging from 0% to 50%. Three samples were evaluated at each concentration of LM. **Figure 3**a presents representative stress–strain curves for silicone composites with images of a ϕ = 50% LMEE sample stretching to 600% strain. From these data, the influence of stiffness of the liquid inclusions is studied by measuring the elastic modulus in the low-strain regime (0–10% strain). Figure 3b shows that as the amount of liquid metal increases from ϕ = 0% to ϕ = 50%, the measured elastic modulus increases from 85 to 235 kPa. As the elastomer and LM are virtually incompressible, the composite is expected to maintain an infinite bulk modulus, i.e., $K_e = K_{LM} = \infty \Rightarrow K^* = \infty \; \forall \phi$. Utilizing Eshelby's theory of composites and assuming incompressible elastic inclusions of modulus E_i dispersed in a solid of modulus E, the composite modulus E^* is:[18,27]

$$E^* = E\frac{1+\frac{2}{3}\frac{E_i}{E}}{\left(\frac{2}{3}-\frac{5\phi}{3}\right)\frac{E_i}{E}+\left(1+\frac{5\phi}{3}\right)} \quad (2)$$

Equation (2) is plotted as a function of ϕ in Figure 3b for different regimes of inclusion stiffness. Three regimes are represented: stiff inclusions (1 MPa < E_i < 1 TPa), soft inclusions (129 kPa < E_i < 1 MPa), and liquid inclusions with surface tension (0 kPa < E_i < 129 kPa). The limit E_i = 129 kPa is based on recent observations by Style et al.[18] that liquid inclusions can stiffen solids and exhibit an effective modulus $E_i = E\{24\alpha/(10 + 9\alpha)\}$, where E is the modulus of the surrounding elastomer, $\alpha = \gamma/ER$, γ is the surface tension of the liquid droplet, and R is the droplet radius. For values of γ = 620 mJ m^{-2}, E = 85 kPa, and R = 5.0 µm, it follows that surface tension and surface stress can effectively make the liquid act as an elastic inclusion with modulus E_i = 129 kPa. However, as observed in Figure 3b, the LMEE composites have stiffnesses above those predicted by this estimate and are instead well within the soft inclusion regime. Specifically, good agreement between the experimental data and Equation (2) is found with an inclusion modulus value of 320 kPa. The larger inclusion modulus value used for fitting could be attributed to both the theory assuming that the particles are noninteracting, which is likely violated at higher volume fractions, and that the oxide

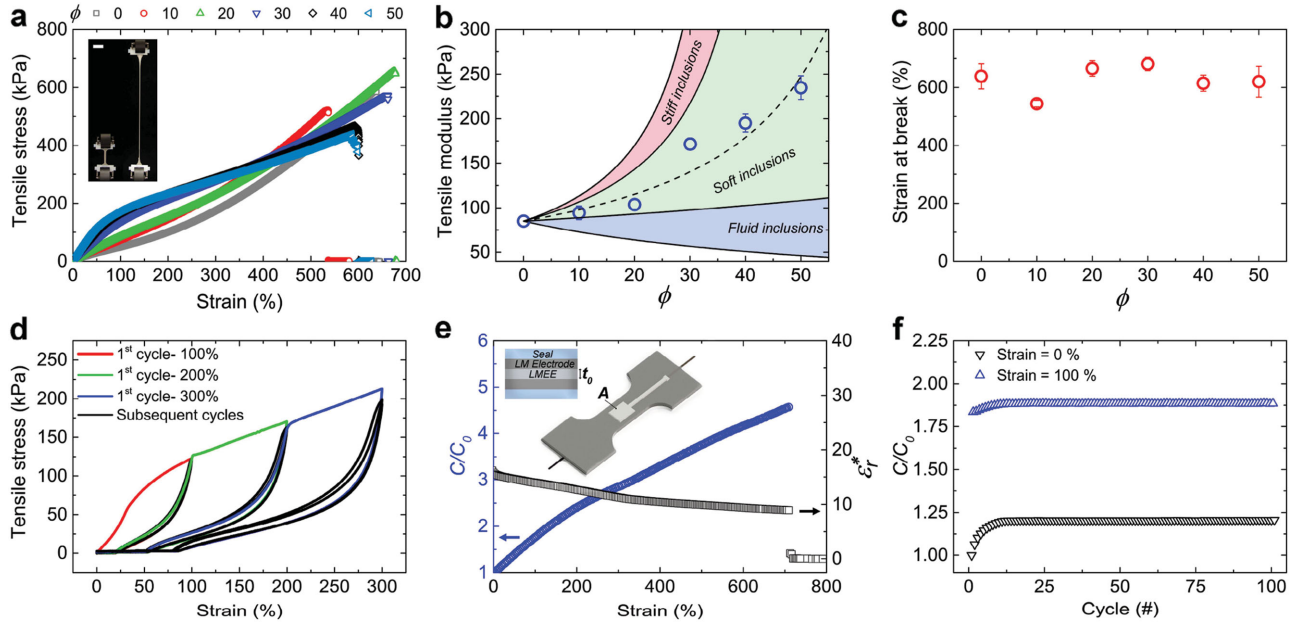

Figure 3. Mechanical and electromechanical characterization of LMEEs. a) Stress versus strain plot for LMEEs from φ = 0% to φ = 50% tested until failure. The image shows the φ = 50% at 0% and 600% strain, scale bar, 25 mm. b) Plot of tensile modulus (measured to 10% strain) as a function of the volume fraction loading of liquid metal (φ); the dashed line is the prediction of Equation (2) showing the increase in modulus due to the liquid-metal inclusions (E_i = 320 kPa). c) Strain at break for the LMEEs as a function of φ. Error bars = ±1 s.d. and error bars smaller than symbol size are omitted. d) Cyclic loading of a φ = 50% LMEE with three cycles at each strain. The materials display a Mullins effect where the initial loading cycle at each strain shows significant hysteresis but subsequent loading cycles show a greatly reduced hysteresis. e) Electromechanical coupling strain to break curve showing the (left axis, blue circles) increase of capacitance (C) relative to the initial capacitance (C_0) and (right axis, black squares) dielectric constant calculated from Equation (3) as a function of stretch. f) Cyclic testing of the LMEE to 100% strain over 100 cycles.

DOI: 10.1002/adma.201506243

skin on the LM drops can also act to stiffen the inclusions.[28] Despite the stiffening effect, the composites are similar in modulus to soft synthetic materials and biological tissue.[1,29]

These LMEE composites are also able to undergo significant deformations. Figure 3c shows that the LMEEs composites are able to stretch to strains on the order of 600%, similar to that of the unfilled elastomer. The composite also exhibits very little hysteresis (Figure 3d) when comparing the loading and unloading curves. This suggests negligible internal friction and losses due to viscoelasticity. The only exception is for the initial load of a freshly prepared (virgin) sample, during which a significant Mullin's effect is observed.[30,31] Such a response to initial loading is typical in elastomer composites and, in the case of LMEEs, vanishes with subsequent loading (unless the sample is stretched beyond its previous maximum strain). The LMEEs were also loaded in compression with a rigid cylindrical indenter of $R = 0.75$ mm and $R = 1.50$ mm up to 6250 N m^{-1} on a rigid glass substrate and continued to be insulating even though the material underwent significant permanent deformation (Figure S5, Supporting Information). These mechanical characteristics highlight the robustness of the LMEEs to extreme deformations which could be expected for stretchable electronics applications.

The electrical response to mechanical deformation is a significant parameter for stretchable dielectrics. Figure 3e,f presents results for the electrical permittivity and electromechanical coupling of EGaIn–silicone composites ($\phi = 50\%$). Measurements are performed on a stretchable parallel-plate capacitor composed of an LMEE dielectric and EGaIn electrodes sealed in an additional layer of silicone (Figure 3e, inset). The normalized capacitance, C/C_0, where C_0 is measured at 0% strain, increases under tensile loading until the dielectric fails at over 700% strain. For a parallel-plate capacitor the initial capacitance can be calculated by $C_0 = \varepsilon_r \varepsilon_0 A_0/t_0$, where $\varepsilon_0 = 8.85 \times 10^{-12}$ F m^{-1} is the vacuum permittivity, and A_0 and t_0 are the initial planar area and thicknesses, respectively. Under the assumption of incompressibility the dielectric constant of the LMEEs during stretching from an initial length L_0 to the instantaneous length L can be calculated as:

$$\varepsilon_r = \frac{Ct_0}{\varepsilon_0 A_0}\frac{1}{\lambda} \tag{3}$$

where $\lambda = L/L_0$ is the extension ratio. Using Equation (3) the dielectric constant is plotted in Figure 3e. It is observed that as the sample is loaded in tension, the capacitance increases by a factor of over 4.5, while the dielectric constant decreases from 18 to 9 when stretched from 0% to 700% strain. To further study the durability of the LMEEs as dielectric materials, we performed cyclic testing experiments to 100% strain under tensile loading over 100 cycles (Figure 3f). During the experiments, the capacitance increased slightly at both 0% and 100% strain during the first 10 cycles, but then remained constant until the test is completed at 100 cycles. The ability to undergo significant strain over 100 cycles without degradation of the electrical or mechanical properties further demonstrates LMEEs as stretchable dielectric materials.

In addition to exploring LMEEs in silicone elastomers, we also investigated their behavior in polyurethane elastomer matrices at high volume loadings ($\phi = 50\%$) (Figure S6 and S7 of the Supporting Information for particle analysis). Compared to the silicone, the polyurethane-based LMEEs have a higher elastic modulus ($E = 780$ kPa) and a lower average strain to break of 182%. However, the dielectric constant of the polyurethane elastomers is found to be greater. Therefore, if extreme strains and moduli on the order of 100–200 kPa are not required, the general strategy developed for silicone LMEEs can be extended to polyurethane elastomers. As seen in **Figure 4**a, the dielectric constant across the frequency range from 1 to 200 kHz for the polyurethane LMEEs at $\phi = 50\%$ is above 42. Additionally, the dissipation factor is below 0.1 (Figure 4b). To connect the measurements from the silicone elastomers and the polyurethane elastomers, and provide a general understanding of LMEEs as dielectric materials we revisit Equation (1). When plotting the silicone and urethane LMEEs on a plot of effective normalized permittivity $\varepsilon_r^*/\varepsilon_{rm}$ versus ϕ at 0% strain we see that the results collapse on a single line described by the theory (Figure 4c). This clearly shows the applicability of LM inclusions for increasing the dielectric constant in hyperelastic media.

Because of their robust mechanical properties and ease of fabrication, the LMEE composites introduced here are an excellent model system for examining the electro-elasticity of more general classes of soft-matter heterogeneous materials. Future efforts will focus on the derivation and experimental

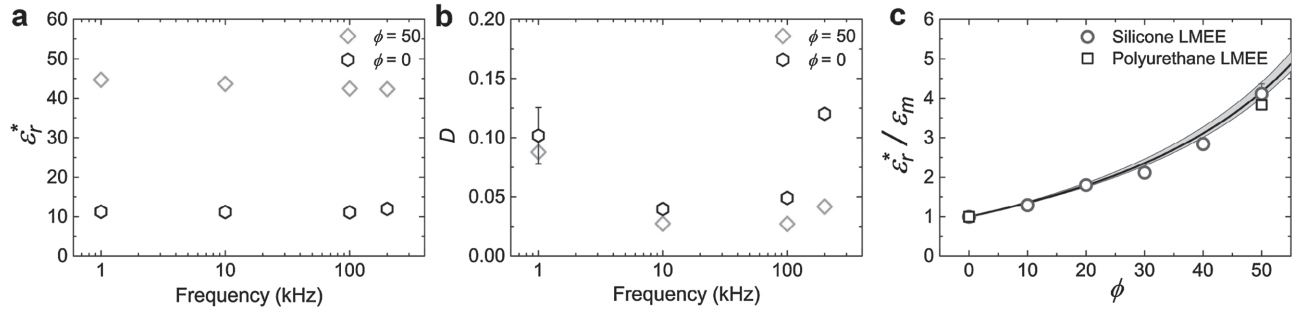

Figure 4. Connecting polyurethane and silicone LMEEs. a) Plot of effective relative permittivity versus testing frequency for polyurethane LMEEs at $\varphi = 0\%$ and $\varphi = 50\%$. b) Plot of dielectric dissipation factor (D) as a function of frequency for the polyurethane LMEEs, showing low dissipation. c) The dielectric performance of the LMEES is generalized by plotting effective normalized permittivity for both the silicone and polyurethane LMEEs, where the data collapse onto a single line described by Equation (1) with $p = 1.49 \pm 0.36$. Error bars = ±1 s.d. and error bars smaller than the symbol size are omitted.

Adv. Mater. **2016**,
DOI: 10.1002/adma.201506243

validation of continuum models based on statistically homogeneous representations of elastomers embedded with randomly shaped and distributed liquid-metal inclusions. These models can then be utilized to better understand the electromechanical coupling behavior for the deformable inclusions presented in this work. Moreover, such theories could potentially be extended to examine the mechanics of other multiphase compositions, e.g., ionic gels, densely packed colloidal suspensions, and soft microfluidic systems with ordered microchannel networks. From an applications' perspective, these materials provide opportunities for integration into soft electronics including sensors and soft energy harvesting devices. In particular, hyperelastic capacitive strain sensors would be able to measure stretches well above double their initial length with significantly improved sensitivity.

Experimental Section

Fabrication: Ecoflex 00–30 and Vytaflex 30 were prepared at a 1:1 weight ratio of part A to part B using an AR-100 THINKY planetary centrifugal mixer. Gallium and indium purchased from Gallium Source, LLC were combined at 75% Ga:25% In by weight to produce EGaIn. The LMEE was then fabricated via shear mixing of the polymer and EGaIn with a mortar and pestle until a viscous emulsion was formed and the droplets appeared to be less than 30 μm under the microscope (≈10 min). For materials with low volume percent EGaIn, a higher concentration sample was prepared first and diluted with the addition of further polymer. The emulsion could then be deposited onto a substrate using a thin film applicator (ZUA 2000.150, Zehntner). Patterning was done using stencil lithography, cutting masks from LaserTape (IKONICS Imaging) with a VLS 3.50 laser cutter (Universal Laser Systems, Inc.). Ease Release 200 was used as a releasing agent for Ecoflex 00–30 based samples, while a 50 μm layer of Sylgard 184 (Dow Corning Corporation) was used for the Vytaflex 30 composite. Once deposited, the material was cured for 16 h at 50 °C.

Nano-CT Scan: 3D imaging on an EGaIn–silicone composite (ϕ = 50%) was performed with a Zeiss Xradia UltraXRM-L200 nano-CT scanner. The instrument settings provided a resolution of 150 nm on a cylindrical sample with a diameter of 62 μm and a scan height of 65 μm. Sample preparation was accomplished by placing a plastic capillary tube with an inner and an outer diameter of 62 and 87 μm, respectively, on top of a needle in a syringe. The capillary tube was then filled with uncured composite material by retracting the syringe plunger. The composite was cured in the capillary tube for 16 h.

Dielectric Measurements: Measurements were performed at room temperature, which was above the melting point of EGaIn (15 °C), by creating a thin film of the LMEEs with a thin film applicator on a metal plate. 1 cm × 1 cm EGaIn contact pads were then applied to the surface of the LMEEs to act as the top plate of the capacitor. Leads were then connected to the supporting metal plate and a wire probe was placed into the EGaIn contact. A benchtop LCR meter (889B; BK Precision) was connected to a PC using the remote interface mode and used to collect data. The capacitance was measured and the permittivity was calculated from these values based on the parallel plate sample geometry. The dissipation factor (D) was calculated by the LCR meter and recorded. Three samples were prepared of each specimen and ten measurements were made on each sample. The data were then averaged together to get a representative data set.

Mechanical Measurements: Mechanical samples were prepared in a dogbone geometry and tested on an Instron 5969 mechanical testing machine with a 10 N load cell. Three samples were tested for each volume percent of LM. The experiments were run at an extension rate of 10 mm min^{-1} and data were collected continuously throughout the experiment until failure for the strain to break samples or when the test was complete for the cyclic testing.

Electromechanical Coupling Measurements: Electromechanical coupling samples were fabricated in layers, using EGaIn to form a stretchable parallel plate capacitor which was encapsulated in polymer. LMEE was first deposited in a dogbone geometry onto a substrate and cured. The EGaIn electrode was then painted onto the LMEE using a stencil, overlapping with a strip of 3M Fabric Tape CN-3490 cut and adhered to an end of the sample. This conductive fabric tape was used to interface the capacitor to external circuits and collect measurements. An acrylic scaffold was placed around the sample and polymer (matching that of the LMEE sample) was poured over the sample to encapsulate the LM electrode. Once cured, the sample was removed from the substrate; another EGaIn electrode was painted onto the bottom side, again overlapping a strip of fabric tape and encapsulated with more polymer.

The samples were clamped into grips with integrated electrical leads on an Instron 5969 mechanical testing machine with a 1 kN load cell and capacitance data were collected with the benchtop LCR meter. The electromechanical coupling data till failure were run at an extension rate of 100 mm min^{-1} and the cyclic testing was conducted at an extension rate of 10 mm min^{-1}.

Supporting Information

Supporting Information is available from the Wiley Online Library or from the author.

Acknowledgements

M.D.B. and A.F. contributed equally to this work. The authors thank the AFOSR Young Investigator Program (Mechanics of Multifunctional Materials and Microsystems; Dr. Les Lee; FA9550-13-1-0123) and NASA Early Career Faculty Award (No. NNX14AO49G) for supporting this research. Mechanical characterization was performed on a materials testing system acquired through an ONR DURIP (Bio-inspired Autonomous Systems; Dr. Tom McKenna; No. N00014140778).

Received: December 15, 2015
Revised: February 17, 2016
Published online:

[1] D.-H. Kim, N. Lu, R. Ma, Y.-S. Kim, R.-H. Kim, S. Wang, J. Wu, S. M. Won, H. Tao, A. Islam, K. J. Yu, T. Kim, R. Chowdhury, M. Ying, L. Xu, M. Li, H.-J. Chung, H. Keum, M. McCormick, P. Liu, Y.-W. Zhang, F. G. Omenetto, Y. Huang, T. Coleman, J. a. Rogers, *Science* **2011**, *333*, 838.
[2] M. Kaltenbrunner, T. Sekitani, J. Reeder, T. Yokota, K. Kuribara, T. Tokuhara, M. Drack, R. Schwödiauer, I. Graz, S. Bauer-Gogonea, S. Bauer, T. Someya, *Nature* **2013**, *499*, 458.
[3] C. Majidi, *Soft Rob.* **2014**, *1*, 5.
[4] R. F. Shepherd, F. Ilievski, W. Choi, S. A. Morin, A. A. Stokes, A. D. Mazzeo, X. Chen, M. Wang, G. M. Whitesides, *Proc. Natl. Acad. Sci. USA* **2011**, *108*, 20400.
[5] S. J. A. Koh, X. Zhao, Z. Suo, *Appl. Phys. Lett.* **2009**, *94*, 262902.
[6] X. Niu, S. Peng, L. Liu, W. Wen, P. Sheng, *Adv. Mater.* **2007**, *19*, 2682.
[7] M. L. Hammock, A. Chortos, B. C. K. Tee, J. B. H. Tok, Z. Bao, *Adv. Mater.* **2013**, *25*, 5997.
[8] Z.-M. Dang, J.-K. Yuan, J.-W. Zha, T. Zhou, S.-T. Li, G.-H. Hu, *Prog. Mater. Sci.* **2012**, *57*, 660.
[9] A. Shakun, *Masters Thesis*, Tampere University of Technology, Tampere, Finland **2014**.
[10] G. Gallone, F. Carpi, D. De Rossi, G. Levita, A. Marchetti, *Mater. Sci. Eng. C* **2007**, *27*, 110.

[11] F. Carpi, D. De Rossi, *IEEE Trans. Dielectr. Electr. Insul.* **2005**, *12*, 835.
[12] L. Bokobza, C. Belin, *J. Appl. Polym. Sci.* **2007**, *105*, 2054.
[13] A. R. Von Hippel, *Dielectric Materials and Applications: Papers by Twenty-Two Contributors*, The Technology Press Of MIT, Cambridge, MA, USA **1954**.
[14] S. Ahmed, F. R. Jones, *J. Mater. Sci.* **1990**, *25*, 4933.
[15] J. Cho, M. S. Joshi, C. T. Sun, *Compos. Sci. Technol.* **2006**, *66*, 1941.
[16] S. Y. Fu, X. Q. Feng, B. Lauke, Y. W. Mai, *Compos., Part B* **2008**, *39*, 933.
[17] A. Fassler, C. Majidi, *Adv. Mater.* **2015**, *27*, 1928.
[18] R. W. Style, R. Boltyanskiy, B. Allen, K. E. Jensen, H. P. Foote, J. S. Wettlaufer, E. R. Dufresne, *Nat. Phys.* **2015**, *11*, 82.
[19] M. F. Ashby, L. J. Gibson, U. Wegst, R. Olive, *Proc. R. Soc. London A* **1995**, *450*, 123.
[20] R. C. Chiechi, E. A. Weiss, M. D. Dickey, G. M. Whitesides, *Angew. Chem. Int. Ed.* **2008**, *47*, 142.
[21] M. D. Dickey, R. C. Chiechi, R. J. Larsen, E. A. Weiss, D. A. Weitz, G. M. Whitesides, *Adv. Funct. Mater.* **2008**, *18*, 1097.
[22] I. D. Joshipura, H. R. Ayers, C. Majidi, M. D. Dickey, *J. Mater. Chem. C* **2015**, *3*, 3834.
[23] C.-W. Nan, R. Birringer, D. R. Clarke, H. Gleiter, *J. Appl. Phys.* **1997**, *81*, 6692.
[24] J. C. M. Garnett, *Philos. Trans. R. Soc. London, A* **1904**, *203*, 385.
[25] D. A. G. Bruggeman, *Ann. Phys.* **1935**, *416*, 636.
[26] T. C. Choy, *Effective Medium Theory: Principles and Applications*, Clarendon Press, Oxford, UK **1999**.
[27] J. D. Eshelby, *Proc. R. Soc. London A* **1957**, *241*, 376.
[28] Q. Xu, N. Oudalov, Q. Guo, H. M. Jaeger, E. Brown, *Phys. Fluids* **2012**, *24*, 063101.
[29] C. Li, G. Guan, R. Reif, Z. Huang, R. K. Wang, *J. R. Soc., Interface* **2012**, *9*, 831.
[30] L. Mullins, *Rubber Chem. Technol.* **1969**, *42*, 339.
[31] J. Diani, B. Fayolle, P. Gilormini, *Eur. Polym. J.* **2009**, *45*, 601.

Adv. Mater. **2016**,
DOI: 10.1002/adma.201506243